JOURNAL OF MATERIALS SCIENCE 35 (2000) 2405–2411

Electrical characteristics of the MOD-derived $SrBi_{2x}Ta_2O_9$ and $SrBi_{2.4}(Ta,Nb)_2O_9$ thin films

DAE JOONG YEON, JOO DONG PARK, YONGWOOK KWON, TAE SUNG OH
Department of Metallurgical Engineering and Materials Science, Hong Ik University, Seoul 121-791, South Korea
E-mail: ohts@wow.hongik.ac.kr

Ferroelectric and leakage current characteristics of the MOD-derived $SrBi_{2x}Ta_2O_9$ ($0.8 \leq x \leq 1.6$) and $SrBi_{2.4}(Ta_{1-y}Nb_y)_2O_9$ ($0 \leq y \leq 1$) thin films were investigated. The SBT and SBTN films were fully crystallized to Bi-layered perovskite structure by annealing at 800 °C for 1 hour in oxygen atmosphere. The ferroelectric characteristics of the SBT films were optimized at the Bi/Ta mole ratio x of 1.2. The leakage current density of the Bi-excess SBT films decreased remarkably by the post-metallization annealing at 800 °C for 10 minutes in oxygen ambient. The ferroelectric characteristics of the SBTN films were optimized with the SBN content y of 0.25. The $SrBi_{2.4}(Ta_{0.75}Nb_{0.25})_2O_9$ film exhibited $2P_r$ and E_c of 19.04 μC/cm^2 and 24.94 kV/cm at ±5 V, which were superior to $2P_r$ of 11.3 μC/cm^2 and E_c of 39.6 kV/cm obtained for the $SrBi_{2.4}Ta_2O_9$ film after the post-metallization annealing. The MOD-derived $SrBi_{2.4}(Ta_{0.75}Nb_{0.25})_2O_9$ film did not exhibit the polarization fatigue after 10^{11} switching cycles at ±5 V.

1. Introduction

Ferroelectric thin films have been extensively investigated for use in nonvolatile memory due to their electrically switchable remanent polarization [1–3]. Lead zirconate titanate (PZT) thin films have been widely investigated to apply for ferroelectric random access memory (FRAM) [1, 4, 5]. However, significant decrease in the remanent polarization after 10^6 switching cycles, i.e., the polarization fatigue, in the Pt/PZT/Pt capacitors has made it difficult to realize the commercial FRAM products with PZT thin films [6, 7]. To overcome the polarization fatigue in the Pt/ferroelectric/Pt capacitors, $SrBi_2Ta_2O_9$-based thin films of Bi-layered perovskite structure have been extensively investigated in recent years [1–3, 8, 9].

Ferroelectric characteristics of the $SrBi_2Ta_2O_9$ films fabricated by metalorganic deposition (MOD) are largely dependent on the Bi content in the MOD coating solution, because vaporization of the Bi oxide occurs during annealing of the $SrBi_2Ta_2O_9$ films at 800 °C. Also, it has been reported that the remanent polarization of the $SrBi_2Ta_2O_9$ thin films can be increased by solid solutioning with other Bi-layered perovskite materials of high polarization and high Curie temperature [7, 10–12]. $SrBi_2Ta_2O_9$ and $SrBi_2Nb_2O_9$ have the same crystal structure and similar lattice parameter, and $SrBi_2Nb_2O_9$ has Curie temperature of 420 °C higher than 310 °C of $SrBi_2Ta_2O_9$ [13]. Thus, $SrBi_2(Ta,Nb)_2O_9$ thin films are expected to exhibit better ferroelectric properties for FRAM applications.

In this study, effects of the Bi content and the post-metallization annealing on the ferroelectric and leakage current characteristics of the MOD-derived $SrBi_{2x}Ta_2O_9$ ($0.8 \leq x \leq 1.6$) thin films have been characterized firstly. Then, the ferroelectric properties of the MOD-derived $SrBi_{2.4}(Ta_{1-y}Nb_y)_2O_9$ ($0 \leq y \leq 1$) thin films have been investigated by substituting Ta oxide with Nb oxide for the $SrBi_{2.4}Ta_2O_9$ composition which exhibited the highest remanent polarization among the MOD-derived $SrBi_{2x}Ta_2O_9$ thin films.

2. Experimental procedure

$SrBi_{2x}Ta_2O_9$ (SBT) and $SrBi_{2.4}(Ta_{1-y}Nb_y)_2O_9$ (SBTN) thin films were prepared on the platinized silicon (100) substrates by MOD process using the Sr-2-ethylhexanate, Bi-2-ethylhexanate, Ta-2-ethyl hexanate, and Nb-2-ethylhexanate as starting materials. To make the SBT and SBTN coating solutions, metal precursors were mixed with Sr : Bi : Ta mole ratio of $1 : 2x : 2$ ($0.8 \leq x \leq 1.6$) and with Sr : Bi : Ta : Nb mole ratio of $1 : 2.4 : 2(1-y) : y$ ($0 \leq y \leq 1$), respectively, and then diluted to 0.05 M concentration with *n*-butyl acetate. SBT and SBTN films were deposited on the $Pt/Ti/SiO_2/Si$ substrates by spin-coating at 3000 rpm for 30 seconds, and spin-coated films were dried at 400 °C for 10 minutes in air. This procedure was repeated several times to obtain the desired film thickness of 400 nm. Finally, the films were annealed at 800 °C for 1 hour in oxygen ambient. Pt top electrodes of 200 μm diameter and 200 nm thickness were sputter-deposited on the SBT and SBTN film surface at room temperature.

Crystalline phase of the SBT and SBTN films was characterized by low-angle X-ray diffractometry (XRD) with incident angle of 5° and microstructure of the films was observed using scanning electron

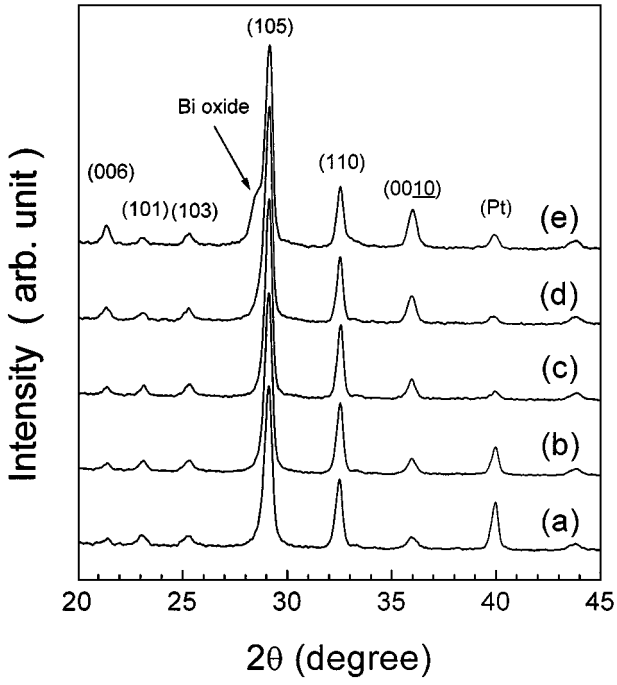

Figure 1 XRD patterns of the $SrBi_{2x}Ta_2O_9$ films with the Bi/Ta mole ratio x of (a) 0.8, (b) 1.0, (c) 1.2, (d) 1.4, and (e) 1.6.

microscopy (SEM). Remanent polarization and coercive field of the SBT and SBTN films were characterized by RT66A ferroelectric tester and leakage current density was measured using HP 4140B semiconductor parameter analyzer. Fatigue test up to 10^{11} switching cycles was performed using a square wave with an amplitude of ± 5 V and a frequency of 1 MHz.

3. Results and discussion

3.1. Characteristics of the $SrBi_{2x}Ta_2O_9$ thin films

Fig. 1 shows the XRD patterns of the SBT thin films after annealing at 800 °C for 1 hour in oxygen atmosphere. All the MOD-derived SBT films were fully crystallized to polycrystalline with almost random orientation regardless of the Bi/Ta mole ratio x ($0.8 \leq x \leq 1.6$). As shown in Fig. 1e, a diffraction peak which could be due to Bi oxide such as Bi_2O_3 [14–16] was observed relatively strongly for the film with the highest Bi/Ta mole ratio x of 1.6.

Fig. 2 shows SEM micrographs of the SBT films with various Bi/Ta mole ratio. The grain size of the SBT films increased with increasing the Bi/Ta mole ratio x, which

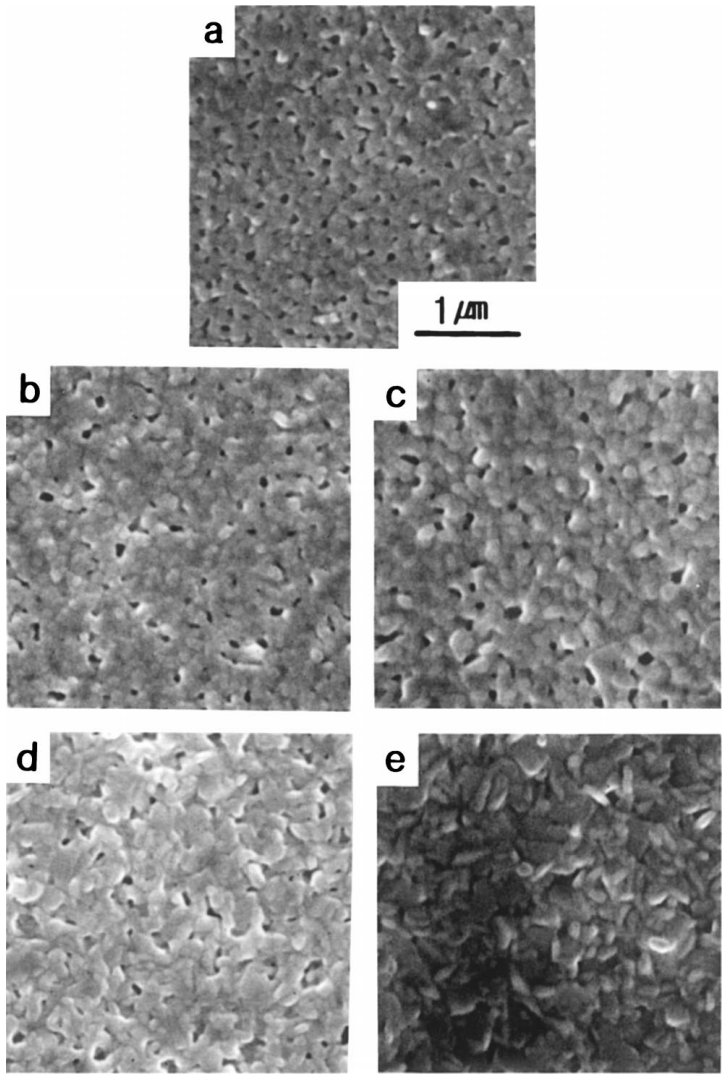

Figure 2 SEM micrographs observed on the surface of the $SrBi_{2x}Ta_2O_9$ films with the Bi/Ta mole ratio x of (a) 0.8, (b) 1.0, (c) 1.2, (d) 1.4, and (e) 1.6.

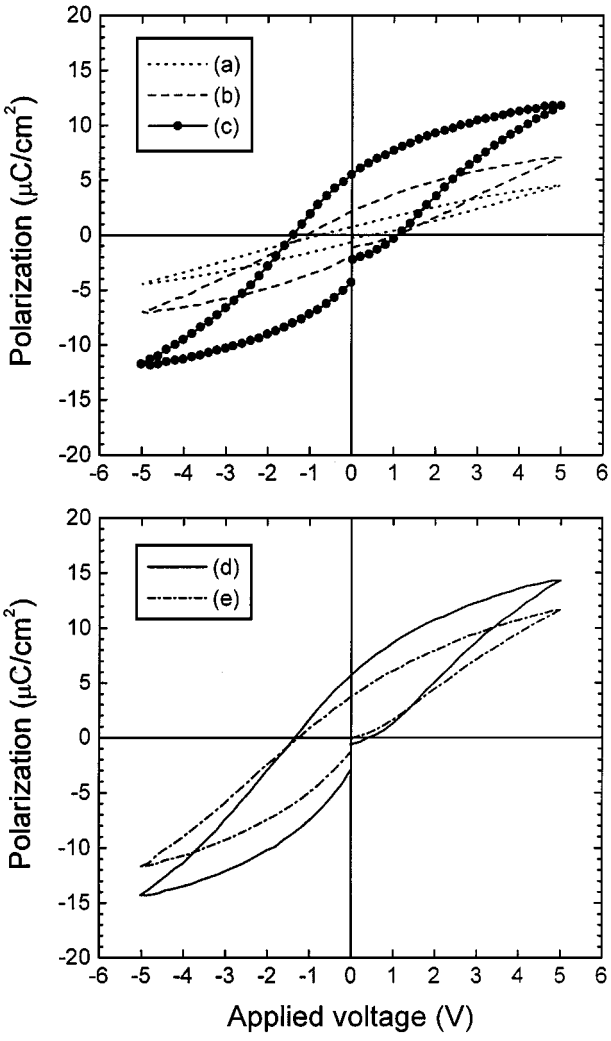

Figure 3 Ferroelectric hysteresis loop of the $SrBi_{2x}Ta_2O_9$ films with the Bi/Ta mole ratio x of (a) 0.8, (b) 1.0, (c) 1.2, (d) 1.4, and (e) 1.6 at applied voltage of ±5 V.

might be attributed to the fact that excess Bi promotes the crystallization of the SBT film from fluorite to Bi-layered perovskite structure [15]. As reported by others [14], the grain shape of the MOD-derived SBT films was also changed with the Bi/Ta mole ratio x. Contrary to the equiaxed grains for the films of $x = 0.8 \sim 1.2$, the elongated rod-like grains have been observed for the films with higher Bi/Ta mole ratio x of 1.4 and 1.6.

Fig. 3 illustrates ferroelectric hysteresis curves of the SBT films measured at applied voltage of ±5 V. With increasing the Bi/Ta mole ratio x up to 1.2, the remanent polarization, coercive field, and the saturation characteristic, i.e., the squareness ratio (remanent polarization/saturation polarization: P_r/P_s) of the SBT films increased. With increasing the excess Bi content further than $x = 1.2$, however, the ferroelectric characteristics of the SBT films became deteriorated. As illustrated in Fig. 4 which shows the remanent polarization ($2P_r$) and coercive field (E_c) of the SBT films measured at ±5 V, the maximum values of $2P_r = 9.79\ \mu C/cm^2$ and $E_c = 24.2$ kV/cm were obtained for the film of $x = 1.2$. Similarly to our results, Watanabe *et al.* [7] and Chen *et al.* [14] have also reported that the maximum remanent polarization of the MOD-derived SBT films was obtained with the Bi-excess composition of $x = 1.2 \sim 1.3$. Chen *et al.* [14] explained the increment of $2P_r$ with the excess Bi content as the grain size effect with the results that the SBT films composed of the grains smaller than a critical size did not exhibit the ferroelectric characteristics and the grain size of the MOD-derived SBT films increased with increasing the excess Bi content.

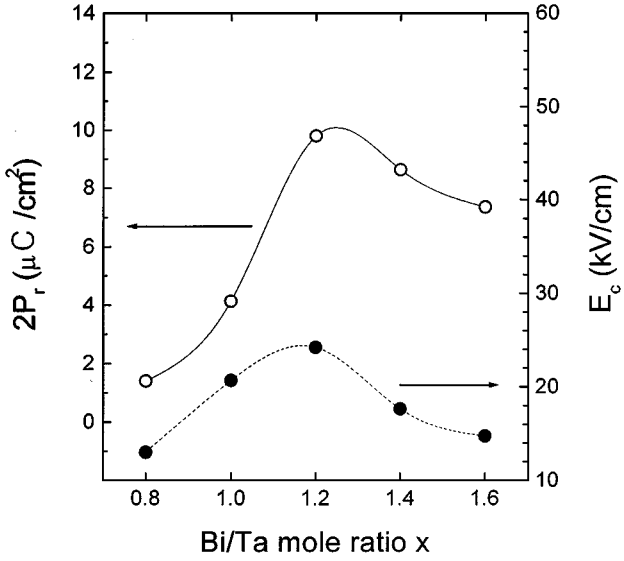

Figure 4 Remanent polarization ($2P_r$) and coercive field (E_c) of the $SrBi_{2x}Ta_2O_9$ films as a function of the Bi/Ta mole ratio.

As shown in Fig. 2, the grain size of the SBT films increased monotonously with increasing the Bi/Ta mole ratio x from 0.8 to 1.6. However, $2P_r$ of the SBT films reached maximum at $x = 1.2$ and then decreased with increasing x further than 1.2. $SrBi_2Ta_2O_9$ may be written as $(Bi_2O_2)^{2+}(SrTa_2O_7)^{2-}$ consisted of two perovskite-like $(SrTa_2O_7)^{2-}$ layers, alternating with a non-ferroelectric layer of $(Bi_2O_2)^{2+}$, along the c-axis [1, 7, 9]. As ferroelectric properties of $SrBi_2Ta_2O_9$ depend on O-Ta-O chains in the perovskite layers, the polarization of $SrBi_2Ta_2O_9$ occurs on the planes perpendicular to c-axis. Thus, the remanent polarization and coercive field of the SBT films decrease significantly with increasing the degree of the c-axis orientation [1, 14, 16]. In this study, the degree of c-axis orientation of the SBT films was estimated as Equation 1 using the intensity ratio of the $(00\underline{1}0)$ diffraction to the dominant (105) diffraction. The $(00\underline{1}0)$ diffraction was the strongest one among the $(00\,\ell)$ diffractions of the SBT films, as shown in Fig. 1.

$$\text{Degree of } c\text{-axis orientation} = \frac{[I_{(00\underline{1}0)}/I_{(105)}]_F}{[I_{(00\underline{1}0)}/I_{(105)}]_P} - 1 \quad (1)$$

In Equation 1, $[I_{(00\underline{1}0)}/I_{(105)}]_F$ is the intensity ratio measured for the SBT films and $[I_{(00\underline{1}0)}/I_{(105)}]_P$ is the intensity ratio reported for $SrBi_2Ta_2O_9$ powder [18]. As shown in Fig. 5, the degree of c-axis orientation of the SBT films increased with increasing the Bi/Ta mole ratio x. Thus, it could be thought that both the grain size effect and the degree of c-axis orientation played roles simultaneously on the variation of $2P_r$ value of the MOD-derived SBT films with the Bi/Ta mole ratio. With increasing the Bi/Ta mole ratio, $2P_r$ increased

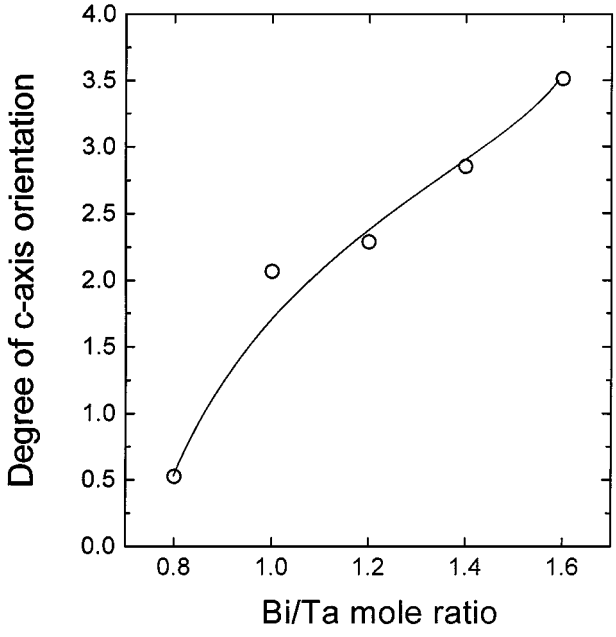

Figure 5 Degree of *c*-axis orientation of the $SrBi_{2x}Ta_2O_9$ films as a function of the Bi/Ta mole ratio.

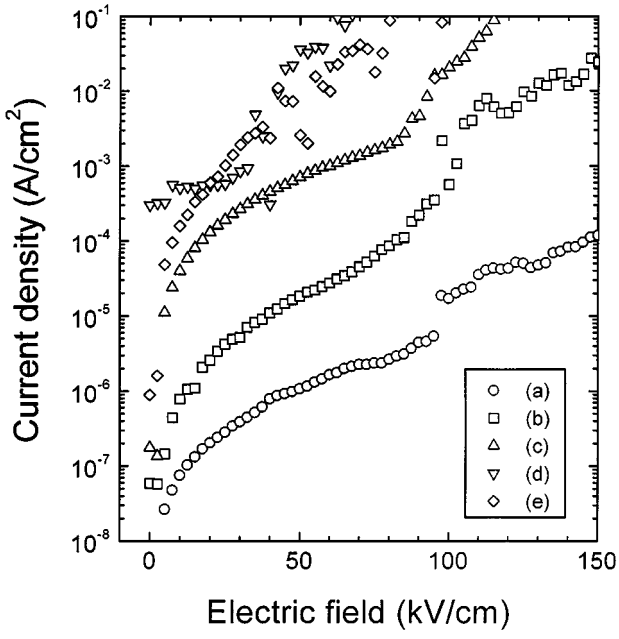

Figure 6 Leakage current density of the $SrBi_{2x}Ta_2O_9$ films with the Bi/Ta mole ratio x of (a) 0.8, (b) 1.0, (c) 1.2, (d) 1.4, and (e) 1.6.

as the grain size became larger. As the degree of *c*-axis orientation increased also with the increase of the Bi/Ta mole ratio, however, $2P_r$ decreased after reaching the maximum at the Bi/Ta mole ratio x of 1.2.

As shown in Fig. 6, the leakage current density of the MOD-derived SBT films increased with increasing the Bi/Ta mole ratio x. This might be caused by the increase of the Pt/SBT interface roughness due to the larger grain size of the SBT film with increasing the excess Bi content [15]. Larger leakage current density at higher Bi/Ta mole ratio could be also attributed to the existence of leaky Bi oxide or metallic Bi at grain boundaries and triple points [14, 15, 17]. To improve the leakage current characteristics of the SBT films, post-metallization annealing of the Pt/SBT/Pt/Ti/SiO_2/Si specimens was performed at 800 °C for 10 minutes in oxygen ambient.

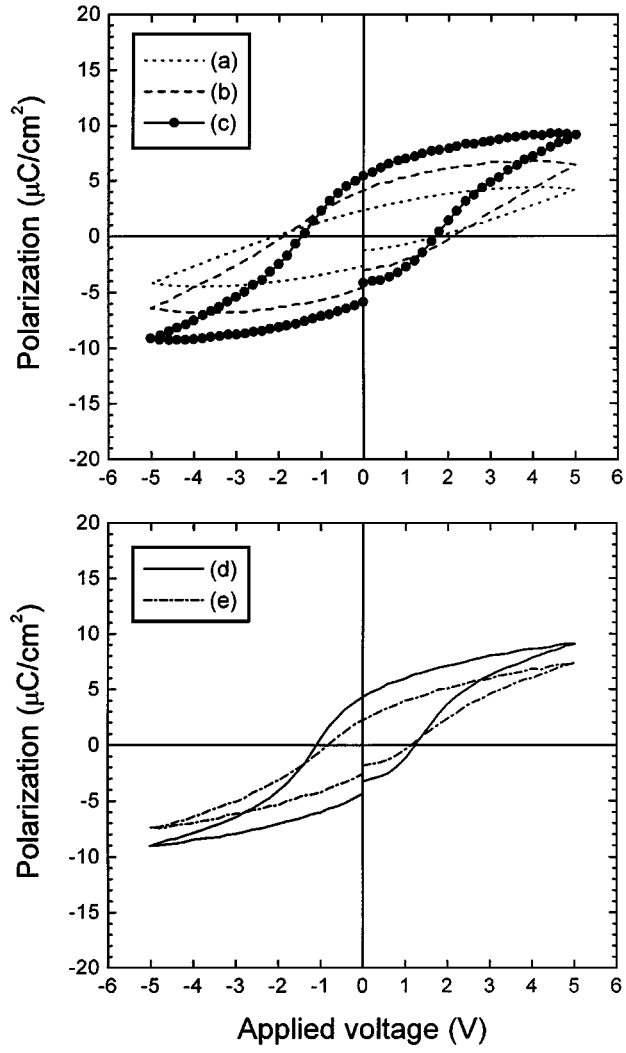

Figure 7 Ferroelectric hysteresis loop of the $SrBi_{2x}Ta_2O_9$ films with the Bi/Ta mole ratio x of (a) 0.8, (b) 1.0, (c) 1.2, (d) 1.4, and (e) 1.6 at ±5 V after the post-metallization annealing.

Fig. 7 shows the ferroelectric hysteresis curves of the SBT films measured at ±5 V after the post-metallization annealing. Compared to the hysteresis curves in Fig. 3, it could be known that the remanent polarization and coercive field of the SBT films increased with the post-metallization annealing for all the Bi/Ta mole ratio x of 0.8 ∼ 1.6. Especially for the films of $x = 1.2$ and $x = 1.4$, the saturation characteristic, i.e., the squareness ratio (P_r/P_s) was greatly improved. After the post-metallization annealing, the optimum ferroelectric characteristics of $2P_r$: 11.3 μC/cm^2 and E_c : 39.6 kV/cm were obtained also for the film of the Bi/Ta mole ratio x of 1.2.

Fig. 8 illustrates the leakage current density of the SBT films after the post-metallization annealing. Effects of the post-metallization annealing on the leakage current density of the SBT films could be clearly seen by comparison of Fig. 8 with Fig. 6. While the leakage current density after the post-metallization annealing increased for the Bi-deficient films with $x \leq 1.0$, it decreased for the Bi-excess films of $x \geq 1.2$. Also, the decrement of the leakage current density with the post-metallization annealing enlarged with increasing the excess Bi content, and the film with the Bi/Ta mole ratio x of 1.6 exhibited lowest leakage current density. For

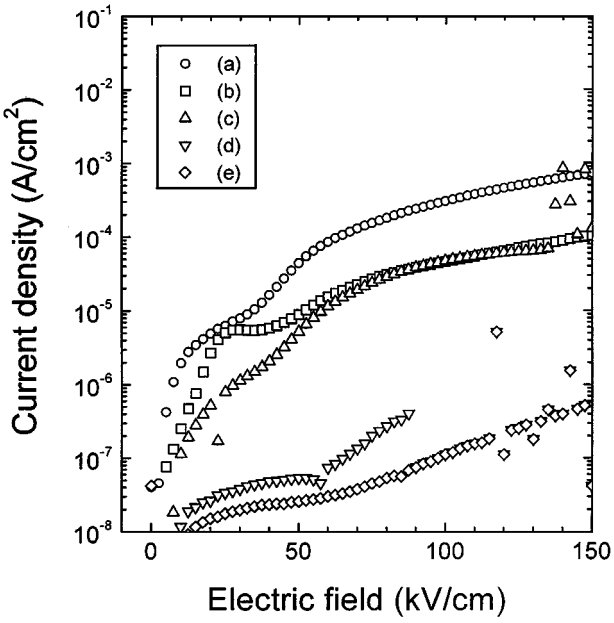

Figure 8 Leakage current density of the $SrBi_{2x}Ta_2O_9$ films with the Bi/Ta mole ratio x of (a) 0.8, (b) 1.0, (c) 1.2, (d) 1.4, and (e) 1.6 after the post-metallization annealing.

the Bi-deficient films, it is not clear yet why the leakage current density increased with the post-metallization annealing. For the Bi-excess films with $x \geq 1.2$, however, the decrease of the leakage current density with the post-metallization annealing could be attributed to the removal of the leaky Bi oxides and also attributed to the interfacial reaction between the SBT film and Pt top electrode [15, 17]. During the post-metallization annealing of the Bi-excess films, leaky Bi oxides such as Bi_2O_3 at the grain boundaries and the triple points were removed by vaporization and diffusion into the SBT lattice [15, 17]. Also, the interface roughness between the top Pt electrode and the SBT film might decrease with interfacial reactions, and micro-voids and defects at the Pt/SBT interface might be eliminated by interdiffusion of Pt and Bi [15, 17], resulting in the decrease of the leakage current density. As can be seen with the comparison of Figs 8 and 6, the decrement of the leakage current density with the post-metallization annealing was larger for the film with higher excess-Bi content, where more interfacial reactions could be expected during the post-metallization annealing. Thus, it might be suggested that the interfacial reactions between Pt top electrode and the SBT film played a dominant role on the decrease of the leakage current density by the post-metallization annealing.

Fig. 9 shows the Auger depth profiles on the $Pt/SrBi_{2.4}Ta_2O_9$ interfaces before and after the post-metallization annealing. After the post-metallization annealing, Bi was observed on top of the Pt top electrode, implying the occurrence of interfacial reactions by interdiffusion of Bi and Pt during the post-metallization annealing.

3.2. Characteristics of the $SrBi_{2.4}(Ta,Nb)_2O_9$ thin films

With the study on the electrical properties of the MOD-derived SBT films, it has been found that the remanent

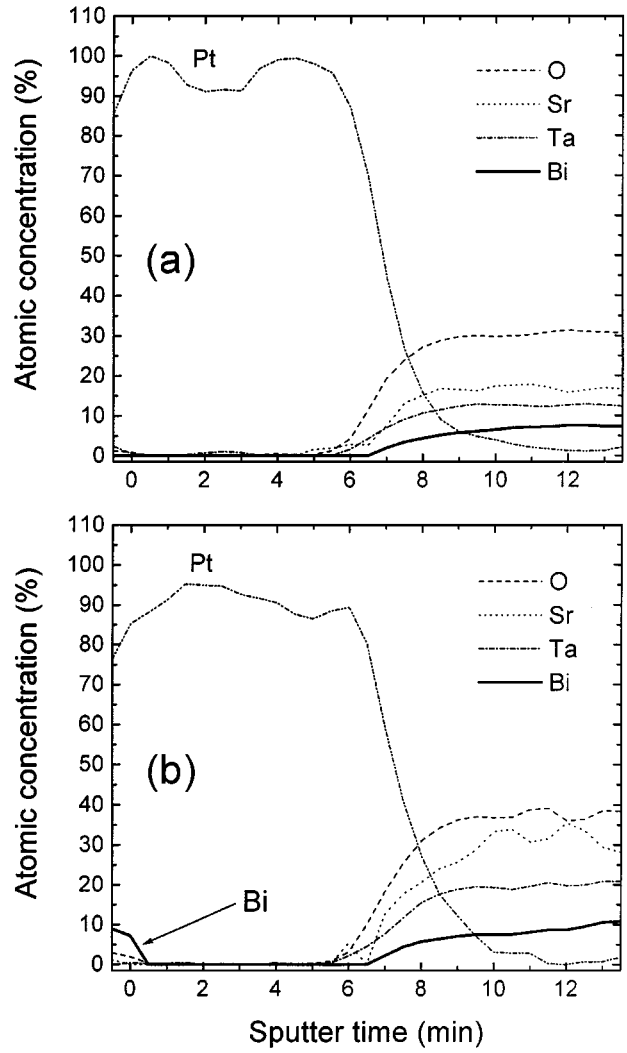

Figure 9 Auger depth profile on the $Pt/SrBi_{2.4}Ta_2O_9$ interfaces (a) before and (b) after the post-metallization annealing.

polarization of the SBT films was optimized at the Bi/Ta mole ratio x of 1.2, and the leakage current characteristics of the Bi-excess SBT films could be improved by the post-metallization annealing. Based on these results, the $SrBi_{2.4}(Ta_{1-y}Nb_y)_2O_9$ films were fabricated using MOD process, and the post-metallization annealing of the films was conducted. Fig. 10 shows the XRD patterns of SBTN thin films after annealing at 800 °C for 1 hour in oxygen atmosphere. The SBTN films were fully crystallized to Bi-layered perovskite structure regardless of the SBN content, indicating that Ta ions were substituted by Nb ions completely in all range of the composition without changing the Bi-layered perovskite structure.

Ferroelectric hysteresis curves of the SBTN thin films after the post-metallization annealing were measured at ±5 V, and illustrated in Fig. 11. While the well-saturated hysteresis curves were obtained for all compositions, the ferroelectric characteristics of the SBTN films were optimized at the composition of $y = 0.25$. At applied voltage of ±5 V, the $SrBi_{2.4}(Ta_{0.75}Nb_{0.25})_2O_9$ film exhibited $2P_r$ and E_c of 19.04 μC/cm^2 and 24.94 kV/cm, respectively, which were superior to $2P_r$ of 11.3 μC/cm^2 and E_c of 39.6 kV/cm obtained for the $SrBi_{2.4}Ta_2O_9$ film after the

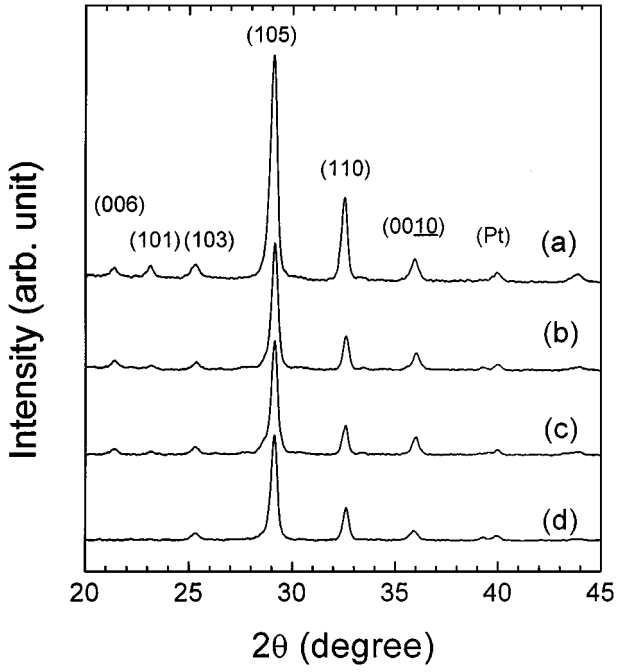

Figure 10 XRD patterns of the $SrBi_{2.4}(Ta_{1-y}Nb_y)_2O_9$ films with the SBN content y of (a) 0, (b) 0.25, (c) 0.4, and (d) 1.0.

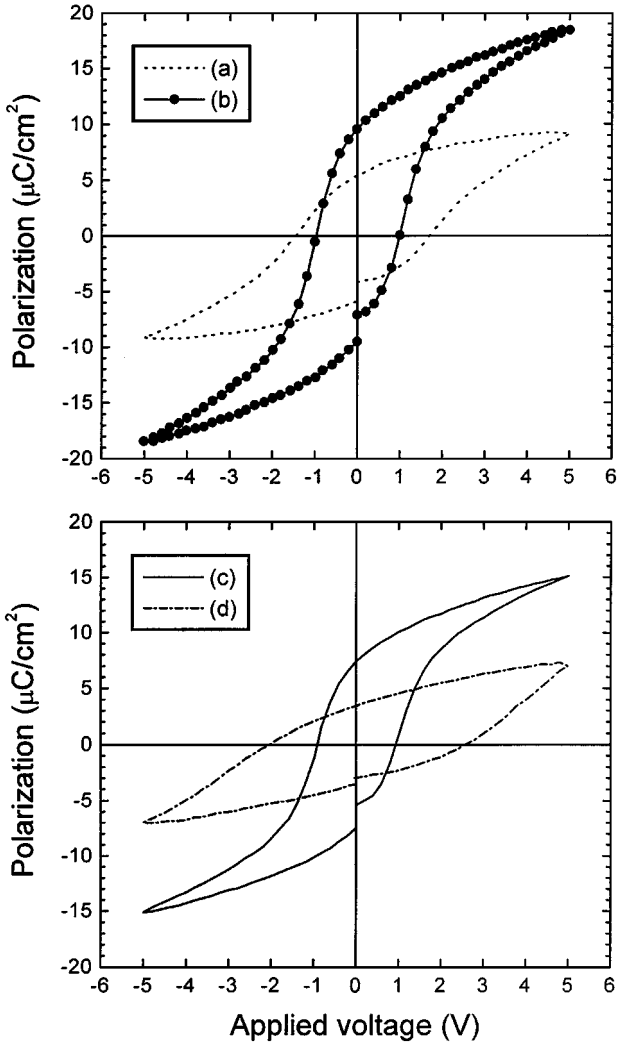

Figure 11 Ferroelectric hysteresis loop of the $SrBi_{2.4}(Ta_{1-y}Nb_y)_2O_9$ films with the SBN content y of (a) 0, (b) 0.25, (c) 0.4, and (d) 1.0 at ±5 V.

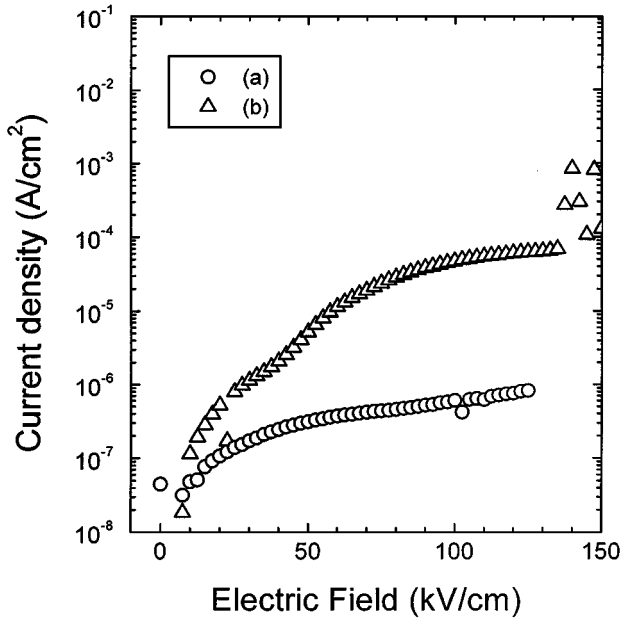

Figure 12 Leakage current density of (a) $SrBi_{2.4}(Ta_{0.75}Nb_{0.25})_2O_9$ film and (b) $SrBi_{2.4}Ta_2O_9$ film.

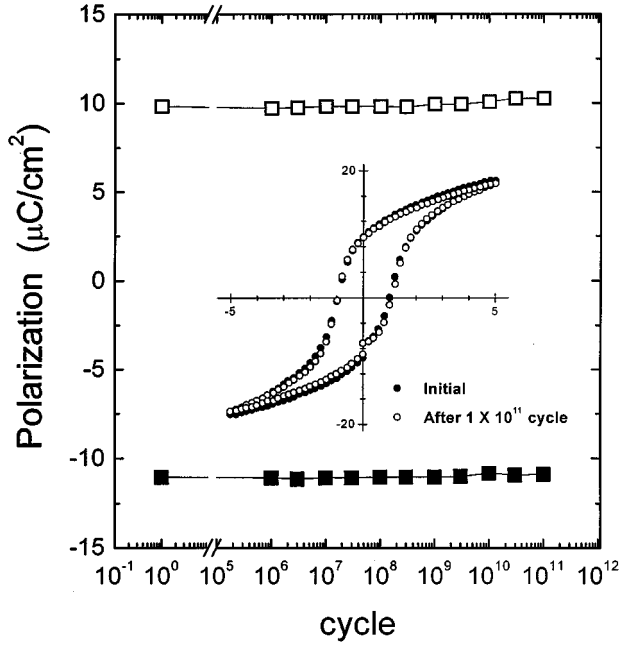

Figure 13 Variation of P_r and $-P_r$ of the $SrBi_{2.4}(Ta_{0.75}Nb_{0.25})_2O_9$ film with the switching cycle at ±5 V.

post-metallization annealing. As shown in Fig. 12, the $SrBi_{2.4}(Ta_{0.75}Nb_{0.25})_2O_9$ film exhibited lower leakage current density ($\leq 10^{-7}$ A/cm^2) up to 75 kV/cm compared to the post-metallization annealed $SrBi_{2.4}Ta_2O_9$ film. As illustrated in Fig. 13, the remanent polarization of the $SrBi_{2.4}(Ta_{0.75}Nb_{0.25})_2O_9$ film was nearly constant after 10^{11} switching cycles at ±5 V, and it can be suggested that the $SrBi_{2.4}(Ta_{0.75}Nb_{0.25})_2O_9$ film is an attractive candidate for FRAM devices.

4. Conclusions

(1) The MOD-derived $SrBi_{2x}Ta_2O_9$ ($0.8 \leq x \leq 1.6$) and $SrBi_{2.4}(Ta_{1-y}Nb_y)_2O_9$ ($0 \leq y \leq 1$) thin films were fully

crystallized to Bi-layered perovskite structure by annealing at 800 °C for 1 hour in oxygen atmosphere.

(2) The ferroelectric characteristics of the SBT film were optimized at the Bi/Ta mole ratio x of 1.2. With increasing the Bi/Ta mole ratio, $2P_r$ increased as the grain size of the SBT films became larger. As the degree of c-axis orientation also increased with the increase of the Bi/Ta mole ratio, however, $2P_r$ decreased after reaching maximum at the Bi/Ta mole ratio x of 1.2. The $SrBi_{2.4}Ta_2O_9$ film exhibited $2P_r$ of 9.79 μC/cm^2 and E_c of 24.2 kV/cm at applied voltage of $\pm$5 V.

(3) The leakage current density of the SBT films increased with increasing the Bi/Ta mole ratio. However, the leakage current density of the Bi-excess SBT films decreased remarkably by the post-metallization annealing at 800 °C for 10 minutes in oxygen ambient, which might be mainly due to the interfacial reactions between the SBT film and Pt top electrode.

(4) The ferroelectric characteristics of the MOD-derived $SrBi_{2.4}(Ta_{1-y}Nb_x)_2O_9$ films were optimized at the composition of $y = 0.25$. The $SrBi_{2.4}(Ta_{0.75}Nb_{0.25})_2O_9$ film exhibited $2P_r$ and E_c of 19.04 μC/cm^2 and 24.94 kV/cm at $\pm$5 V, which were superior to $2P$r of 11.3 μC/cm^2 and E_c of 39.6 kV/cm obtained for the $SrBi_{2.4}Ta_2O_9$ film after the post-metallization annealing. The MOD-derived $SrBi_{2.4}(Ta_{0.75}Nb_{0.25})_2O_9$ film did not exhibit the polarization fatigue after 10^{11} switching cycles at $\pm$5 V.

Acknowledgement

This work was supported by Korea Research Foundation (Project No: 1998-015-D00124).

References

1. J. F. SCOTT and C. A. ARAUJO, *Science* **246** (1989) 1400.
2. C. A. ARAUJO, J. D. CUCHIARO, L. D. MCMILLAN, M. C. SCOTT and J. F. SCOTT, *Nature* **374** (1995) 627.
3. D. J. YEON, J. D. PARK and T. S. OH, *J. Kor. Phys. Soc.* **30** (1998) S173.
4. C. V. R. VASCANT KUMAR, R. PASCUAL and M. SAYER, *J. Appl. Phys.* **71** (1992) 864.
5. S. B. DESU and D. P. VIJAY, *Mater. Sci. Eng.* **B32** (1995) 75.
6. T. MIHARA, H. WATANABE and C. A. ARAUJO, *Jpn J. Appl. Phys.* **33** (1994) 3996.
7. H. WATANABE, T. MIHARA, H. YOSHIMORI and C. A. ARAUJO, *ibid.* **34** (1995) 5240.
8. S. B. REN, C. J. LU, J. S. LIU, H. M. SHEN and Y. N. WANG, *Phys. Rev.* **B54** (1996) 337.
9. H. TABATA, H. TABAKA and T. KAWAI, *Jpn. J. Appl. Phys.* **34** (1995) 5146.
10. X. ZHANG, P. GU and S. B. DESU, *Mat. Res. Soc. Symp. Proc.* **493** (1998) 215.
11. J. ZHU, X. ZHANG, Y. ZHU and S. B. DESU, *J. Appl. Phys.* **83** (1998) 1610.
12. S. D. DESU, P. C. JOSHI, X. ZHANG and S. O. RYU, *ibid.* **71** (1997) 1041.
13. W. PEREZ, E. CHIANG-PARADO, A. REYNES-FIGUEROA, R. S. KATIYAR, D. RAVICHANDRAN and A. S. BHALLA, *Mat. Res. Soc. Symp. Proc.* **493** (1998) 237.
14. T. CHEN, T. LI, X. ZHANG and S. B. DESU, *J. Mater. Res.* **12** (1997) 1569.
15. I. KOIWA, K. TANI, J. MITA and T. IWABUCHI, *Jpn. J. Appl. Phys.* **37** (1998) 192.
16. I. KOIWA, Y. OKADA, J. MITA, A. HASHIMOTO and Y. SAWADA, *ibid.* **36** (1997) 5904.
17. S. Y. CHEN, X. F. CHEN and I. W. CHEN, *Mat. Res. Soc. Symp. Proc.* **361** (1994) 15.
18. J. S. LEE, H. H. KIM, H. J. KWON and Y. W. JWONG, *Appl. Phys. Lett.* **73** (1998) 166.

Received 28 June
and accepted 14 October 1999